



Politecnico  
di Bari

Repository Istituzionale dei Prodotti della Ricerca del Politecnico di Bari

Experimental study of a vertical jet in a vegetated crossflow

This is a pre-print of the following article

*Original Citation:*

Experimental study of a vertical jet in a vegetated crossflow / Ben Meftah, M., De Serio, F., Malcangio, D., Mossa, M., Petrillo, A.F.. - In: JOURNAL OF ENVIRONMENTAL MANAGEMENT. - ISSN 0301-4797. - STAMPA. - 164:(2015), pp. 19-31. [10.1016/j.jenvman.2015.08.035]

*Availability:*

This version is available at <http://hdl.handle.net/11589/452> since: 2021-04-08

*Published version*

DOI:10.1016/j.jenvman.2015.08.035

Publisher:

*Terms of use:*

(Article begins on next page)

# Experimental Study of a Vertical Jet in a Vegetated Crossflow

Mouldi Ben Meftah<sup>a\*</sup>, Francesca De Serio<sup>a</sup>, Daniela Malcangio<sup>a</sup>, Michele Mossa<sup>a</sup>, Antonio Felice Petrillo<sup>a</sup>

<sup>a</sup>Department of Civil, Environmental, Building Engineering and Chemistry, Technical University of Bari, Via E. Orabona 4, 70125 Bari, Italy: e-mail [mouldi.benmeftah@poliba.it](mailto:mouldi.benmeftah@poliba.it)

[francesca.deserio@poliba.it](mailto:francesca.deserio@poliba.it), [daniela.malcangio@poliba.it](mailto:daniela.malcangio@poliba.it), [michele.mossa@poliba.it](mailto:michele.mossa@poliba.it), [antoniofelice.petrillo@poliba.it](mailto:antoniofelice.petrillo@poliba.it)

\*Corresponding author: ph.: +39 080 5963508, fax: +39 080 5963414, e-mail: [mouldi.benmeftah@poliba.it](mailto:mouldi.benmeftah@poliba.it)

## Abstract

Aquatic ecosystems have long been used as receiving environments of wastewater discharges. Effluent discharge in a receiving water body via single jet or multiport diffuser, reflects a number of complex phenomena, affecting the ecosystem services. Discharge systems need to be designed to minimize environmental impacts. Therefore, a good knowledge of the interaction between effluents, discharge systems and receiving environments is required to promote best environmental management practice.

This paper reports innovative 3D flow velocity measurements of a jet discharged into an obstructed crossflow, simulating natural vegetated channel flows for which correct environmental management still lacks in literature. In recent years, numerous experimental and numerical studies have been conducted on vegetated channels, on the one hand, and on turbulent jets discharged into unvegetated crossflows, on the other hand. Despite these studies, however, there is a lack of information regarding jets discharged into vegetated crossflow. The present study aims at obtaining a more thorough understanding of the interaction between a turbulent jet and an obstructed crossflow. In order to achieve such an objective, a series of laboratory experiments was carried out in the Department of Civil, Environmental, Building Engineering and Chemistry of the Technical University of Bari - Italy. The physical model consists of a vertical jet discharged into a crossflow, obstructed by an array of vertical, rigid, circular and threaded steel cylinders. Analysis of the measured flow velocities shows that the array of emergent rigid vegetation significantly affects the jet and the ambient flow structures. It reduces the mean channel velocity, allowing the jet to penetrate higher into the crossflow. It significantly increases the transversal flow motion, promoting a major lateral spreading of the jet within the crossflow. Due to the vegetation array effects, the jet undergoes notable variations in his vortical structure. The variation of the flow patterns affects the mixing process and consequently the dilution of pollutants discharged in receiving water bodies.

Keywords: jet; vegetated crossflow; velocity distribution, jet penetration height, jet spreading, environmental impacts.

## 1. Introduction

Environmental management and sustainable development actually become a common activity of more efficient use of natural resources, forming a key driver of innovation and growth. As an example, Daly (1990) proposed some fundamental principles of sustainable development, one of them, which is in line with the present study, is: “*the emissions released by production and consumption processes should not exceed the absorption and regeneration capacities of the ecosystems*”. In order to achieve such an objective, with wastewater discharges in receiving water bodies, a good knowledge of the interaction between the effluents, the discharge system and the receiving environments is required. For example, aquatic vegetation in natural receiving water bodies strongly affects the ambient flow structures as well as of a discharged wastewater flow, affecting, in turn, the rate of nutrient/contaminant transport and diffusion.

Because of their numerous practical applications, ranging from the discharge of effluents into the atmosphere and water bodies to combustion and thrust control, turbulent jets have been widely analytically, computationally and experimentally studied for several decades (e.g., Ben Meftah et al., 2004; Eroglu and Breidenthal, 1998; Jirka and Harleman, 1979; Morton and Ibbetson, 1996; Muppidi and Mahesh, 2007; Quinn, 2006; Rajaratnam, 1976; Richard and Weston, 1978; Toffolon and Serafini, 2013). In fact, it is fundamental the role that turbulent jets play as the initial mixing phase for pollutants discharged into an environmental receiving body (e.g., river, stream, lake, sea, atmosphere). It is worth mentioning that the discharge of wastewaters into a crossflow, via single jet or multiport diffuser, buoyant or non-buoyant jets, reflects a number of complex phenomena. These include visual deflection and oscillation of jet trajectories, some visualized actions such as mixing of the jet, vortex pair formation within the jet, secondary reverse flow behind the jet and inhibition of jet buoyancy caused by stratified constriction (Yang and Hwang, 2001). The initial jet characteristics (e.g., nozzle shape, dimensions, submerged port height and flow rate), the boundary conditions (e.g., topography, bathymetry, physical properties) and the hydrodynamic features of the cross current (e.g., depth, flow rate, stratification, wave motion), as mentioned in previous studies (e.g., Fischer et al., 1979; Mossa, 2004a and b; Smith and Mungal, 1998), strongly affect the jet mixing processes. Turbulent jets have been widely studied because of their mixing properties. Therefore, an understanding of the jet basic mixing mechanisms could have significant importance for both the engineering control design and the environmental management/monitoring sectors.

A jet in a crossflow is defined as the flow field where a jet of fluid enters and interacts with a crossflowing fluid. The most obvious feature of a jet in a crossflow, as observed by Andreopoulos and Rodi (1984), is the mutual deflection of both the jet and the crossflow. The jet is bent over by the cross-stream, while the latter (crossflow) is deflected as it encounters a rigid obstacle. Consequently, the jet interacts with the deflected flow and entrains fluid from it. With a large ratio of jet to ambient velocities, the jet is only weakly affected near the exit and vertically penetrates into the cross-stream before bending over.

Pathak et al. (2006) indicated that the whole flow field of a jet in a crossflow is characterized by four main vortical structures: (i) shear layer vortices which form at the interface between the jet and the crossflow and have been attributed to Kelvin-Helmholtz type instabilities; (ii) horseshoe vortices due to the adverse pressure gradient upstream of the jet; (iii) wake vortices form at the inner part of the jet; and (iv) counter-rotating vortex pairs (CRVP) form at the cross plane just after the jet hole, becoming as dominant structures downstream in the flow field. (Fig. 1).

Sherif and Pletcher (1989), conducting laboratory measurements on a vertical turbulent jet in crossflow, found two mean velocity maxima on each vertical profile. An absolute maximum which is located within the jet field and corresponds to the jet velocity axis and a local maximum appears in the wake-like region. Pratte and Baines (1967), using flow visualization to determine the jet trajectories and its flow widths within the ambient flow, found that the jet length scales are properly normalized by the factor  $r_{ja}D$ , where  $r_{ja} = U_0/U_a$  is defined as the initial jet to ambient velocity ratio,  $U_0$  is the initial jet velocity,  $U_a$  is the ambient velocity and  $D$  is the jet nozzle diameter.

Vegetation in main channels strongly affects the flow turbulence structures (e.g., Ben Meftah and Mossa, 2013; Ben Meftah et al., 2014). Hydraulic engineers have studied water flow through vegetation to better model sediment and contaminant transport. Field observations demonstrate that submerged and emerged vegetation can baffle local currents and dampen wave energy by providing additional source of drag associated with the plant stems and branches (Nepf et al., 1997). Vegetation also affects the turbulence intensity and then the diffusion process. Because wake turbulence is generated at the stem scale (Nepf, 1999; Poggi et al., 2004; Wilson and Shaw, 1997), the dominant turbulent length scale is shifted downward, relative to unvegetated channel flows (Nepf et al., 1997). Raupach and Thom (1981) and Worcester (1995) indicated that, in vegetated channel, the turbulence production reduces with the reduction of the flow velocity.



The channel is equipped with a side-reservoir spillway with adjustable height in order to maintain a constant and uniform water head. An upstream and a downstream movable gates (made of Plexiglas) are used to define the flow depth and mean velocity in the channel. At the downstream end of the channel, water is intercepted by a rectangular reservoir which is 3 m long, 1 m wide and 1 m deep, equipped with a triangular weir (V-notch sharp crested weir) to measure the channel flow rate.

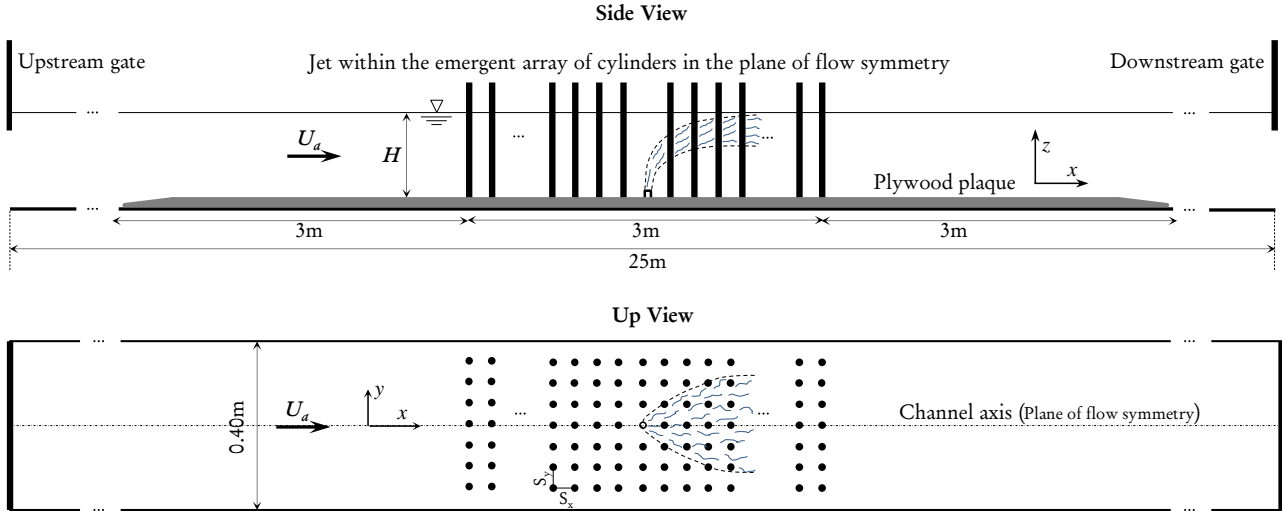


**Fig. 2.** Definition sketch of the jet in the channel with the array of cylinders.

The model array is constructed of vertical, rigid, circular and threaded steel cylinders. The cylinder height,  $h$ , and diameter,  $d$ , are 0.31 m and 0.003 m, respectively. The cylinder extremities are inserted into a plywood plaque 3.0 m long, 0.398 m wide and 0.02 m thick, which in turn was fixed along the channel bottoms, forming the canopy area. The plywood plaque is extended 3 m both upstream and downstream of the array of cylinders (experimental area) and is tapered to the channel bottom to minimize flow disturbance. Cylinders are arranged regularly and spaced longitudinally,  $s_x$ , and transversally,  $s_y$ , with the same distance  $s_x = s_y = \Delta S = 5.0$  cm, so that the cylinder density,  $n$ , was 400 cylinders/m<sup>2</sup>.

The jet-nozzle is placed at the centre of the experimental area, 15.0 m and 0.2 m far from the inlet and the side-walls of the channel, respectively. It is consisted of a circular metallic pipe of diameter  $D = 0.003$  m. The jet is discharged normally to the horizontal channel bottom and upward toward the free water surface. The jet port height  $z_0$ , defined as the vertical distance from the channel bottom surface to the jet nozzle, was 0.03 m. Therefore, we considered  $x = 0$ ,  $y = 0$  and  $z = 0.03$  m as the Cartesian coordinates at the jet-nozzle centre, with  $x$ -,  $y$ - and  $z$ -coordinates denoting the longitudinal, lateral and vertical directions, respectively. The jet is connected to a rectangular fibreglass tank by means of a plastic pipe. The tank is 1.0 m long, 0.5 m wide and 0.5 m deep and is positioned at a height of 3.6 m over the channel bottom surface (for further details see Mossa, 2004a; b). In order to maintain a constant jet discharge, water is continuously pumped into the fibreglass tank by an electro-pump of a discharge greater than the jet discharge. The water excess, overcoming the side-tank spillway, is driven via a pipeline to reach another reservoir from where the water was pumped. The jet discharge is measured using two flow meters; one measures a flow rate ranging between 0 and 100 l/h, while the other one measures a flow rate ranging between 100 and 500 l/h (Fig. 2).

Because water is forced to move around the stems, the flow within the canopy is both three-dimensional and highly heterogeneous at the scale of the individual stem. Therefore, the instantaneous three-dimensional flow velocity components, through different longitudinal, cross and horizontal planes (Fig. 3), were measured accurately using a three-dimensional (3D) Acoustic Doppler Velocimeter (ADV) system, together with CollectV software for data acquisition and

ExploreV software for the data analysis, all produced by Nortek. The ADV was used with a velocity range equal to  $\pm 0.30$  m/s, a velocity accuracy of  $\pm 1$  %, a sampling rate of 25 Hz, a sampling volume of vertical extend of 9 mm and a time of acquisition of 7 minutes. A 15 db signal-to-noise ratio (SNR) and a correlation coefficients larger than 70 % are recommended by the manufacturer for high-resolution measurements. The acquired data were filtered based on the Tukey's method and the bad samples (SNR < 15 db and correlation coefficient < 70 %) were also removed. Because of the configuration of the ADV of downlooking probe, the uppermost 7 cm of the flow could not be sampled (Ghisalberti and Nepf, 2004).

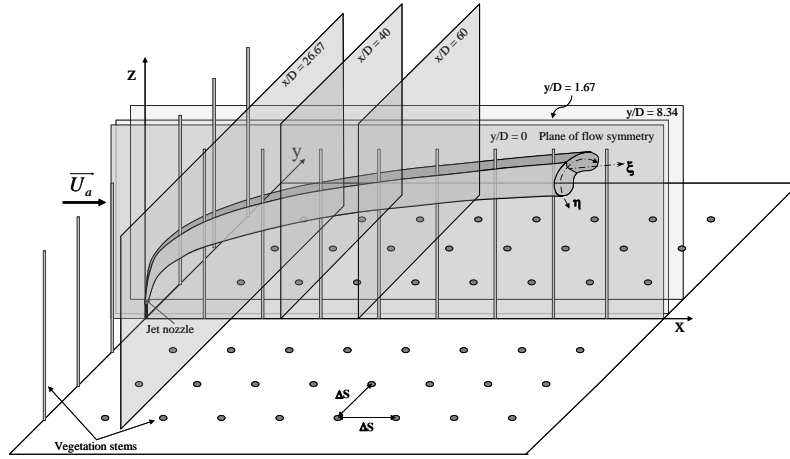


**Fig. 3.** 3D Scheme of the longitudinal and the cross planes where the flow velocity measurements were taken. For the sake of clarity, only the longitudinal row of cylinders, in the plane of flow symmetry, and that in the transversal plane at  $x/D = 0$  are shown, the other rods are simply indicated by the gray points.

Three scenarios of experiments were carried out: (i) the first scenario consists of a jet discharge into an unobstructed channel flow, with the objective to know the jet structure without canopy effects, and refers to runs CJ1 to CJ4, (ii) the second scenario investigates an obstructed channel by an array of cylinders, but without jet, in order to understand the canopy effects on the main ambient flow, and refers to runs CV1 and CV2, and (iii) the third scenario combines between the first and the second scenarios, examining a jet discharge into an obstructed channel flow, and refers to runs CJV1 to CJV4. The initial experimental conditions and parameters are illustrated in Table 1. Herein,  $H$  is the ambient flow depth,  $T$  is the water temperature,  $Fr_a$  is the channel Froude number,  $Fr_0$  is the initial jet Froude number,  $Re_a$  is the channel Reynolds number and  $Re_0$  is the initial jet Reynolds number.

**Table 1.** Initial conditions and parameters of the different experimental runs.

	Runs	$H$ (cm)	$U_a$ ( $\text{ms}^{-1}$ )	$U_0$ ( $\text{ms}^{-1}$ )	$T$ ( $^{\circ}\text{C}$ )	$r_{ja}$ (-)	$Fr_a$ (-)	$Fr_0$ (-)	$Re_a$ (-)	$Re_0$ (-)
<b>Channel Jet</b>	<b>CJ1</b>	37	0.16	5.90	11.3	37.36	0.083	34.38	16036	13845
	<b>CJ2</b>	30	0.19	5.90	14.9	30.29	0.113	34.38	20383	15437
	<b>CJ3</b>	37	0.16	3.93	16.7	24.91	0.083	22.92	18802	10822
	<b>CJ4</b>	30	0.19	3.93	15.5	20.20	0.113	22.92	20733	10468
<b>Channel Cylinder Array</b>	<b>CV1</b>	37	0.16	#	22.0	#	0.083	#	21517	#
	<b>CV2</b>	30	0.19	#	24.0	#	0.113	#	25698	#
<b>Channel Jet Cylinder Array</b>	<b>CJV1</b>	37	0.16	5.90	25.0	37.36	0.083	34.38	23054	19904
	<b>CJV2</b>	30	0.19	5.90	25.0	30.29	0.113	34.38	26282	19904
	<b>CJV3</b>	37	0.16	3.93	28.0	24.91	0.083	22.92	24591	14154
	<b>CJV4</b>	30	0.19	3.93	25.0	20.20	0.113	22.92	26282	13270

# indicates without jet

### 3. Results and Discussion

#### 3.1. Jet penetration within the ambient flow

Velocity measurements in the plane of flow symmetry are useful in determining the jet penetration within the crossflow, which has been one of the primary objectives of many experimental and theoretical studies on this topic. It is well known that the jet velocity decays rapidly as going further downstream of the jet source, reaching the ambient flow velocity. In the current study, extensive measurements of the flow velocity in the plane of flow symmetry, ( $x$ - $z$ ) of  $y/D = 0$ , were taken for runs CJ1 to CJ4 (jet discharge into the unobstructed channel flow). For the jet discharged into the obstructed/vegetated channel (runs CJV1 to CJV4), and due to the limited displacement of the ADV probe between in-line cylinders, the velocity measurements were taken along the plane parallel to the plane of flow symmetry at  $y/D = 8.34$ . Fig. 4 and Fig. 5 show vector maps of the flow velocity  $V_{xz}$  (resultant of the streamwise  $U$  and vertical  $W$  time-average velocity components) of runs CJ1 to CJ4, in the plane of flow symmetry, and those of runs CJV1 to CJV4, in the plane of  $y/D = 8.34$ , respectively. It can be noted that the flow field is well described by the measured velocity vectors and the jet penetration within the ambient flow is clearly shown.

Fig. 4 shows that the jet penetration height within the ambient flow significantly changes from a run to another. The jet axis,  $\xi$  indicated by the dash-dotted line, and the jet vertical width, indicated by a gray spot, are qualitatively plotted for all runs in Fig. 4. The jets with the highest values of  $r_{ja}$ , i.e., CJ1 and CJ2, penetrate deeper into the crossflow and gradually bend over, showing the largest widths in the plane of flow symmetry. At lower values of  $r_{ja}$ , however, i.e., CJ3 and CJ4, the jet is bent over more rapidly within the ambient flow, showing the smallest widths. A comparison between the flow velocity fields of runs CJ1 to CJ4 highlights that the jet width and penetration height increase as  $r_{ja}$  increases.

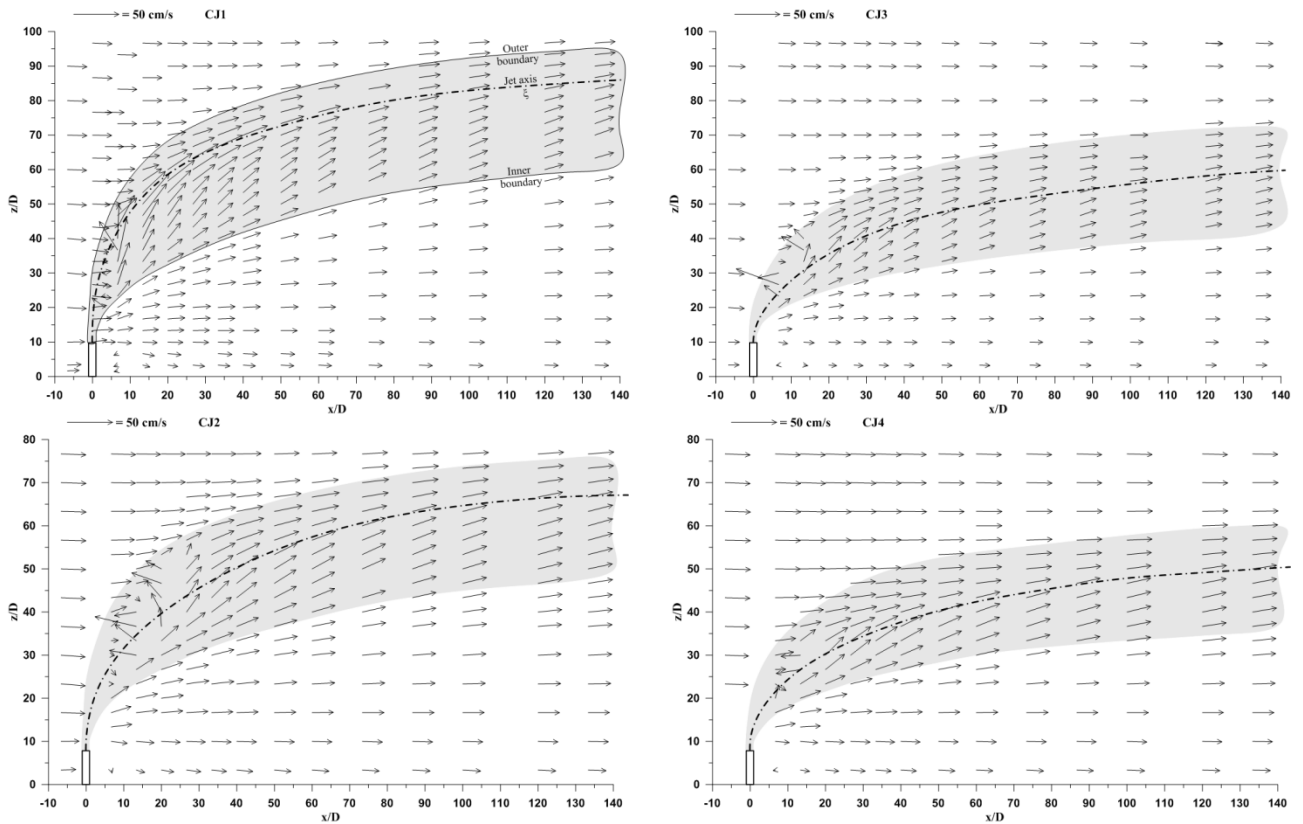


**Fig. 4.** Resultant velocity,  $V_{xz}$ , distribution in the plane of flow symmetry ( $y/D = 0$ ). The jet width and its velocity axis are also qualitatively shown.

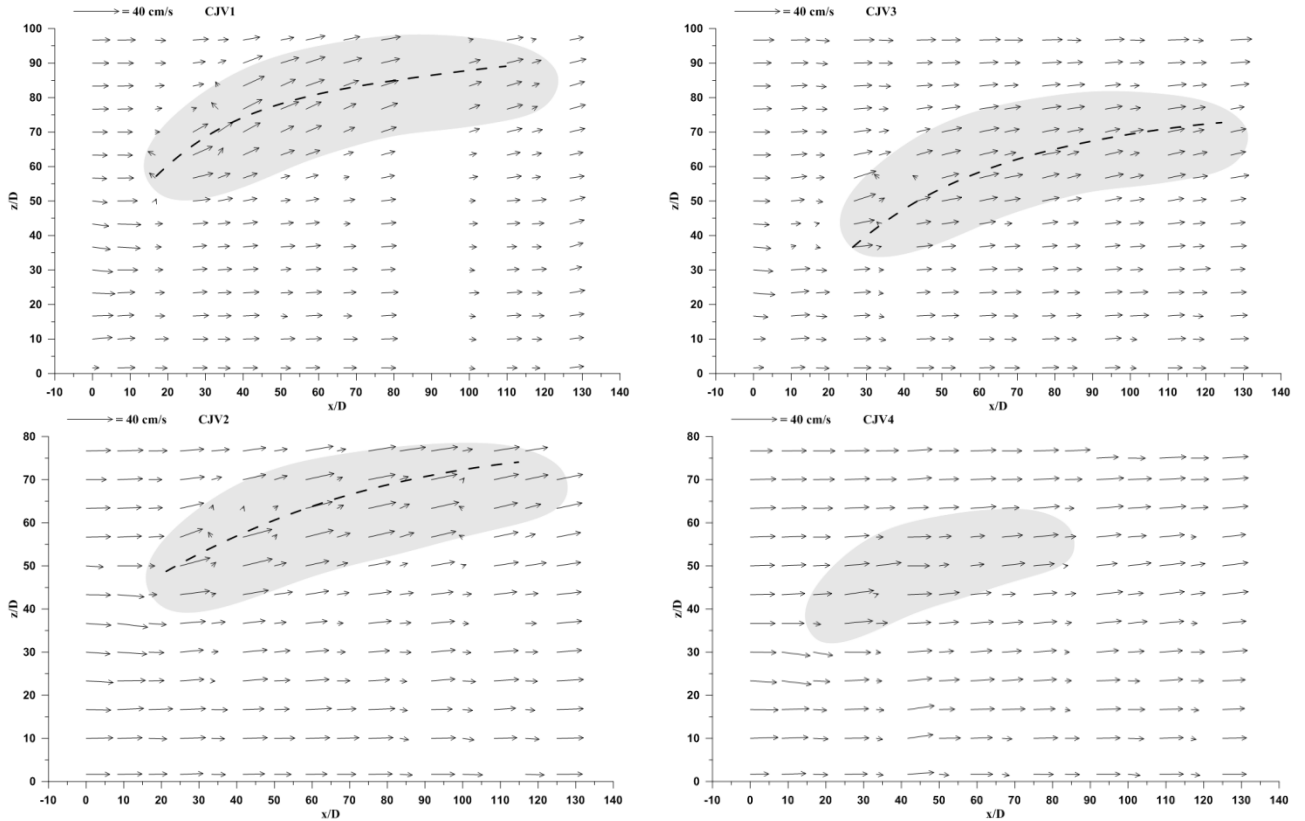


**Fig. 5.** Resultant velocity,  $V_{xz}$ , distribution in the vertical plane at  $y/D = 8.34$ . The regions where the jet is pronounced are marked by the gray spots.

Despite the lateral position of the plane of flow measurements at a distance of  $y/D = 8.34$ , Fig. 5 clearly shows the array effects on the jet structure. This is manifested by a disturbance of the flow velocity  $V_{xz}$ , where a change of its direction and magnitude are evidently observed, as highlighted by the gray spots. On Fig. 5 we also qualitatively plot the position curves of the maximum values of  $V_{xz}$ , as shown by the dash-dotted line. The comparison between Fig. 4 and Fig. 5 show that the curves of maximum  $V_{xz}$ , for runs CJV1 to CJV4, are always higher compared to the jet axes of runs CJ1 to CJ4. This is more pronounced comparing runs CJ1 and CJ2 to CJV1 and CJV2, respectively. This result clearly indicates that, under the same hydraulic conditions, the jet penetrates higher in the obstructed channel flow than in the unobstructed one.

The jet trajectory is one of the most important parameters of a jet discharged into a crossflow. In the present study, the jet trajectory is defined as the locus of the maximum values of the resultant velocity  $V_{xz}$  in the plane of flow symmetry (Rajaratman, 1976), as previously shown in Fig. 4. It is worth mentioning that in literature some confusion is found regarding the jet axis and the jet centreline trajectory definition. Some researchers define the jet trajectory as the locus of maximum jet velocity, while others use the streamline emanating from the centre of the jet (New et al., 2006). Since the jet port height is  $z_0 = 0.03$  m (see the experimental set-up section), in Fig. 6 the dimensionless vertical coordinate is defined as  $(z-z_0)/D$ . Fig. 6(a) shows the jet axes (at  $y/D = 0$ ) plotted in the dimensionless coordinates  $(z-z_0)/D$  versus  $x/D$ . Data refer to runs CJ1 to CJ4 (jets in the unobstructed channel). In addition to the jet axes, the trajectories of the locus of the maximum velocity  $V_{xz}$  of runs CJV1 to CJV3 (jets in the obstructed channel), obtained in the vertical plane ( $x-z$ ) of  $y/D = 8.34$ , are also plotted in Fig. 6(a). The data of run CJV4 are not illustrated in Fig. 6(a), because the jet is less pronounced at the lateral position  $y/D = 8.34$ , due to its smallest cross-section width.

Fig. 6(a) clearly shows the dependence of the jet penetration within the ambient flow on the velocity ratio  $r_{ja}$  (Table 1). The greater the values of  $r_{ja}$ , the greater the jet penetration height. This dependence on  $r_{ja}$  is observed with the jet in the unobstructed channel flow as well as with the jet in

the obstructed one. As well known in literature (e.g., Rajaratman, 1976), in unobstructed channel flows, the vertical position  $z/D$  of the maximum values of  $V_{xz}$  in a jet cross-section shows its greatest value in the plane of flow symmetry ( $y/D = 0$ ) and decreases on moving away from it. This is due to the development of the familiar kidney-shape of the jet cross-section, downwardly concaved, as below shown in Fig. 9. In Fig. 6(a), it can be clearly noted that the trajectories, representing the locus of the maximum velocity  $V_{xz}$  of runs CJV1 to CJV3 at  $y/D = 8.34$ , are located higher than the jet axes of runs CJ1 to CJ4. This evidently confirms the notable increase of the jet penetration height in the obstructed channel flow.

Although the scaling of transversal jet trajectories in an unobstructed crossflow has been the subject of numerous experimental and analytical investigations, there is still no accepted scaling parameter for the jet trajectory (New et al., 2006). Therefore, a data scattering of the jet axes/centrelines is almost always observed in different previous studies. According to Hasselbrink and Mungal (2001), this data scattering is partly due to the definitions of the jet axes and partly from opinions on the best form of the correlating equation. Keffer and Baines (1963) found that, based on their experimental data of a velocity ratio  $r_{ja}$  ranges between 2 to 10 and normalizing the coordinates by  $r_{ja}^2 D$ , i.e.,  $x/r_{ja}^2 D$  and  $z/r_{ja}^2 D$ , the jet trajectories, as defined by the flow streamlines, fall onto a single curve for  $r_{ja} = 6$  to 10, while the data for  $r_{ja} = 2$  to 4 did not collapse well. Kamotani and Greber (1972) proposed an alternative scaling, normalizing the coordinates by  $D$ , i.e.,  $x/D$  and  $z/D$ , and went on to obtain a power-law of the jet trajectories in the form of

$$\frac{z}{D} = A \left( \frac{x}{D} \right)^B \quad (1)$$

where  $A$  and  $B$  are experimental coefficients. Margason (1968) reviewed several correlations and concluded that much of the data could be collapsed by normalizing coordinates with the product  $r_{ja}D$ , leading to a simple power-law trajectory in the form of

$$\frac{z}{r_{ja}D} = A \left( \frac{x}{r_{ja}D} \right)^B \quad (2)$$

The similar power-law in Equation (2) was also proposed by Pratte and Baines (1967), based on their dimensional analysis for a jet of  $r_{ja}$  ranges between 5 and 35. New et al. (2006) indicated that some researchers affirmed that the jet trajectories are best scaled with  $r_{ja}D$ , instead of  $D$  or  $r_{aj}^2 D$ . Moreover, they noted that many of the published experimental data can be converted to the form in Equation (2). Although, there is spread in the values of  $A$  and  $B$  because of the different definitions used to identify the jet trajectory.

Fig. 6(b) shows the jet axis of runs CJ1 to CJ4 scaled with  $r_{ja}D$ , as shown by Equation (2), together with the locus of maximum  $V_{xz}$ , obtained in the plane at  $y/D = 8.34$ , of runs CJV1 to CJV3. In addition to the experimental data of the current study, in Fig. 6(b) we also plot some predicted and experimental jet trajectories obtained in previous studies (Chochua et al., 2000; Kamotani and Greber, 1972; Margason, 1968; Pratte and Baines, 1967; Richard and Weston, 1978). Fig. 6(b) shows that the jet trajectories of runs CJ1 to CJ4 exhibit an almost linear trend with the same slope. The jet trajectories of runs CJ1 and CJ2, on the one hand, and of runs CJ3 and CJ4, on the other hand, tend to collapse onto a single line, showing a slight vertical drop between them. This slight scattering between data implies that the scaling with the product  $r_{ja}D$  is a good way but is not sufficient, as also affirmed in preceding studies (e.g., Hasselbrink and Mungal, 2001; New et al., 2006). Despite the slight data scattering, the jet trajectories, obtained in the unobstructed channel flow of the current study, are globally in good agreement with those obtained by Chochua et al. (2000), Kamotani and Greber (1972), Margason (1968) and Richard and Weston (1978). The

predicted trajectory proposed by Pratte and Baines (1967) appears somewhat higher than the other trajectories.

Fig. 6(b) also indicates that the locus of maximum  $V_{xz}$  of runs CJV1 to CJV3 appear higher than the jet axis of runs CJ1 to CJ4, again confirming that the presence of the array of cylinders/vegetation allows the jet to penetrate higher into the crossflow.

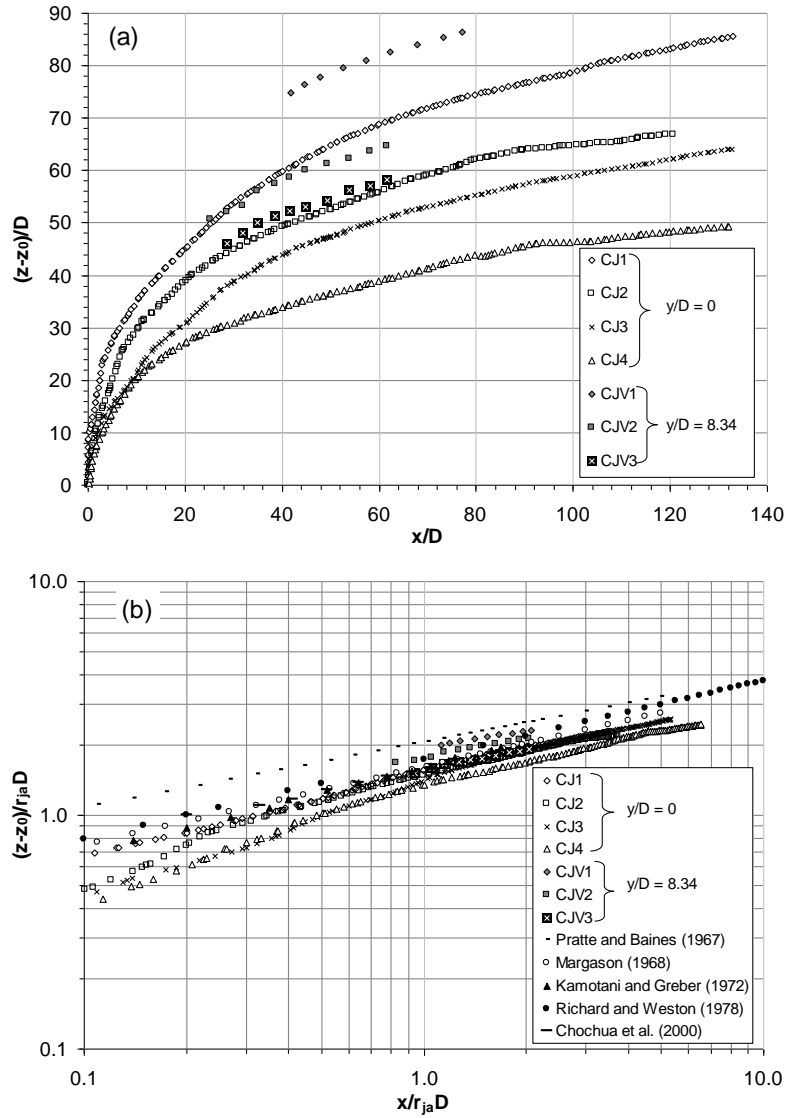


Fig. 6. Jet velocity axis: (a) coordinates are normalized by  $D$ , (b) coordinates are normalized by  $r_{ja}D$ .

### 3.2. Effects of the cylinders/vegetation array on the ambient flow structures

Obstruction of the channel mean flow by an array of cylinders/vegetation creates significant effects on the flow hydrodynamic structure (e.g., Ben Meftah and Mossa, 2013; Ben Meftah et al., 2014; White and Nepf, 2007). Due to these additional effects the jet behaviour becomes more complex and less predictable. In order to better understand how the jet interacts with the obstructed flow, it was useful to firstly study the array impact on the ambient flow without jet, and then we examine the jet behaviour within the array of cylinders.

Fig. 7 shows a map of vectors of the velocity  $V_{xy}$  (resultant of the components  $U$  and  $V$  of the flow velocity) for run CV1, in the horizontal plane ( $x$ - $y$ ) of  $z = 0.5H$ , where  $V$  is the time-averaged transversal velocity component. Fig. 7 clearly indicates that, behind and around each cylinder/rod, the velocity vectors experience notable effects. Close to the rods, their magnitude significantly decrease and their directions undergo considerable deviations relative to the mean stream direction.

Just behind the rods, highly heterogeneous and vortical flow velocity structure takes place, confirming the formation of the well-known wake regions (e.g., Kang, 2003; Nepf, 1999; Nepf, 2004; Williamson, 1985). This result is remarkably consistent with a spatial snapshot of a dye concentration distribution reported by Poggi and Katul (2008).

Fig. 7 shows that, at the downstream positions of  $x = 26.7d$  and  $41.67d$ , the effect of the cylinders on the flow structures considerably reduces. The vectors become slightly deviated relative to the mean flow direction and their amplitudes experience an almost sinusoidal variation as a function of  $y/d$  (Ben Meftah and Mossa, 2013). On the other hand, the more we get closer to the position of a lateral row of cylinders the more the velocity profiles undergo significant impact from the cylinders, and the sinusoidal trend vanishes. At  $x = 16.7d$  and  $33.4d$ , the velocity profiles show small values in the measurement points close to the rods. The largest values, however, are observed at the midway points between two side-by-side rods, giving rise to a flow which behaves like a plume. Fig. 7 indicates that the behaviours of the velocity profiles shown at and downstream of the first lateral row of cylinders repeated in a roughly similar way to the second row. This implies that the velocity profiles are periodic in  $x$  with a period which appears equal to  $\Delta S$  (Ben Meftah and Mossa, 2013). In addition, an examination of Fig. 7 clearly demonstrates the flow symmetry relative to the channel axis, as also observed by Poggi and Katul (2008). Ben Meftah and Mossa (2013), based on the flow  $U$ -velocity distribution, at the downstream position  $x$  where  $U$  undergoes the sinusoidal trend, proposed an empirical expression capable to predict the bulk drag coefficient  $\overline{C_D}$  due to the array of cylinders. Fig. 7 also shows that  $V_{xy}$  is considerably decreased along the plane of flow symmetry ( $y/d = 0$ ), due to the presence of a row of in-line cylinders at this position. Since the jet nozzle ( $x/d = 0, y/d = 0$ ) is also aligned with the same row of cylinders and is of diameter equal to the cylinder diameter ( $D = d$ ), the jet flow effectively undergoes the local effect of cylinders. The significant reduction of the ambient flow velocity, due to the additional resistance generated by the array of cylinders, could be behind the increase of the jet penetration height within the obstructed channel (CJV1 to CJV4).

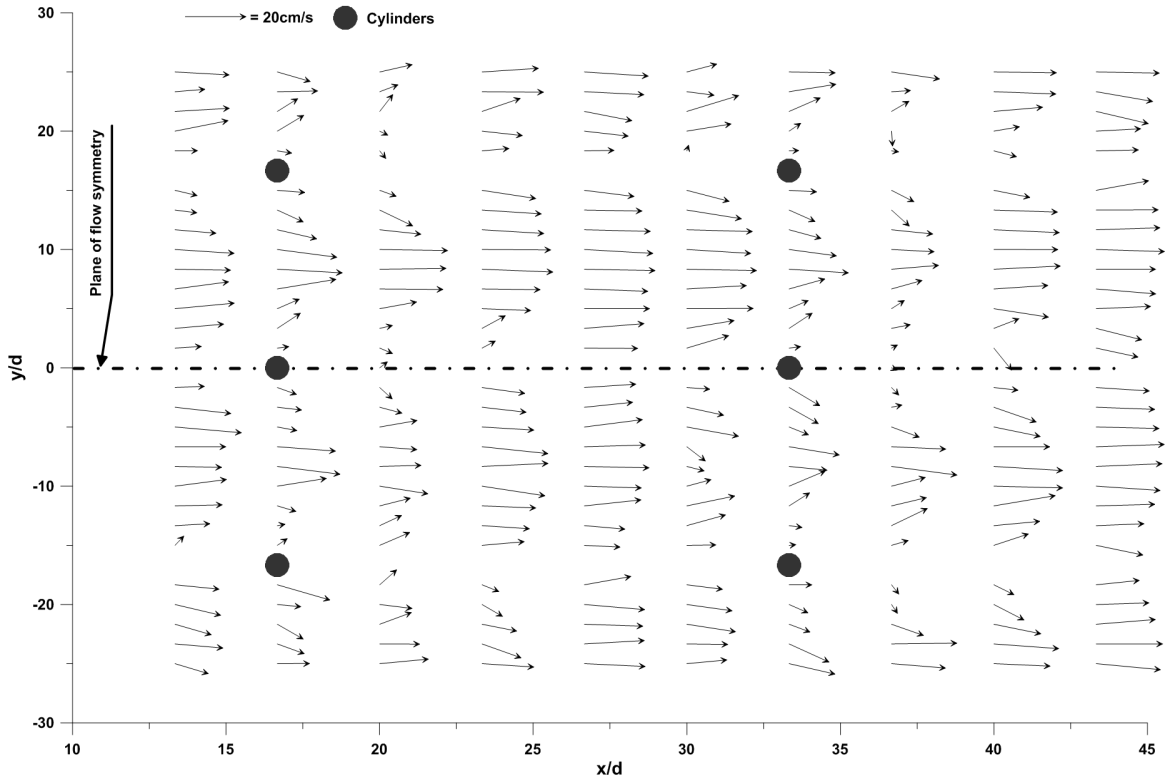


**Fig. 7. Cylinders effect on  $V_{xy}$ -velocity distribution in the horizontal plane at  $z = 0.5H$ , run CV1. The length of the figure axes  $x/d$  and  $y/d$  are displayed in scale (2.6:1). The jet nozzle is positioned at  $(x/d = 0, y/d = 0)$ .**

### 3.3. Effects of the cylinders/vegetation array on the jet flow

With the aim to highlight the significant effects of the cylinder array on the jet flow, in Fig. 8 we compare some vertical profiles of the dimensionless velocity  $V_{xz}/U_a$  between jets discharged into the unobstructed channel (CJ1 to CJ4) and jets discharged into the obstructed/vegetated channel (CJV1 to CJV4) at different downstream positions  $x/D$ . The velocity vertical profiles of runs CJ1 to CJ4 were obtained in the plane of flow symmetry ( $y/D = 0$ ), while those of runs CJV1 to CJV4 were obtained in the plane parallel to the plane of flow symmetry, at  $y/D = 8.34$ . The velocity profiles clearly show the jet penetration within the ambient flow for the different runs, manifested by the sharp increase of  $V_{xz}/U_a$  over a certain vertical distance  $z/D$ . Fig. 8 indicates that the vertical position of the peak of  $V_{xz}/U_a$  always appears higher with runs CJV1 to CJV4 compared to CJ1 to CJ4, respectively. Usually, as also mentioned before, at a lateral position of  $8.34D$  from the plane of flow symmetry, the locus of the peak of  $V_{xz}/U_a$  should be down the jet axis position (at  $y/D = 0$ ), due to the jet kidney-shaped cross-section. This finding again confirms that the jet is much more penetrated within the ambient flow in the obstructed channel rather than the unobstructed one.

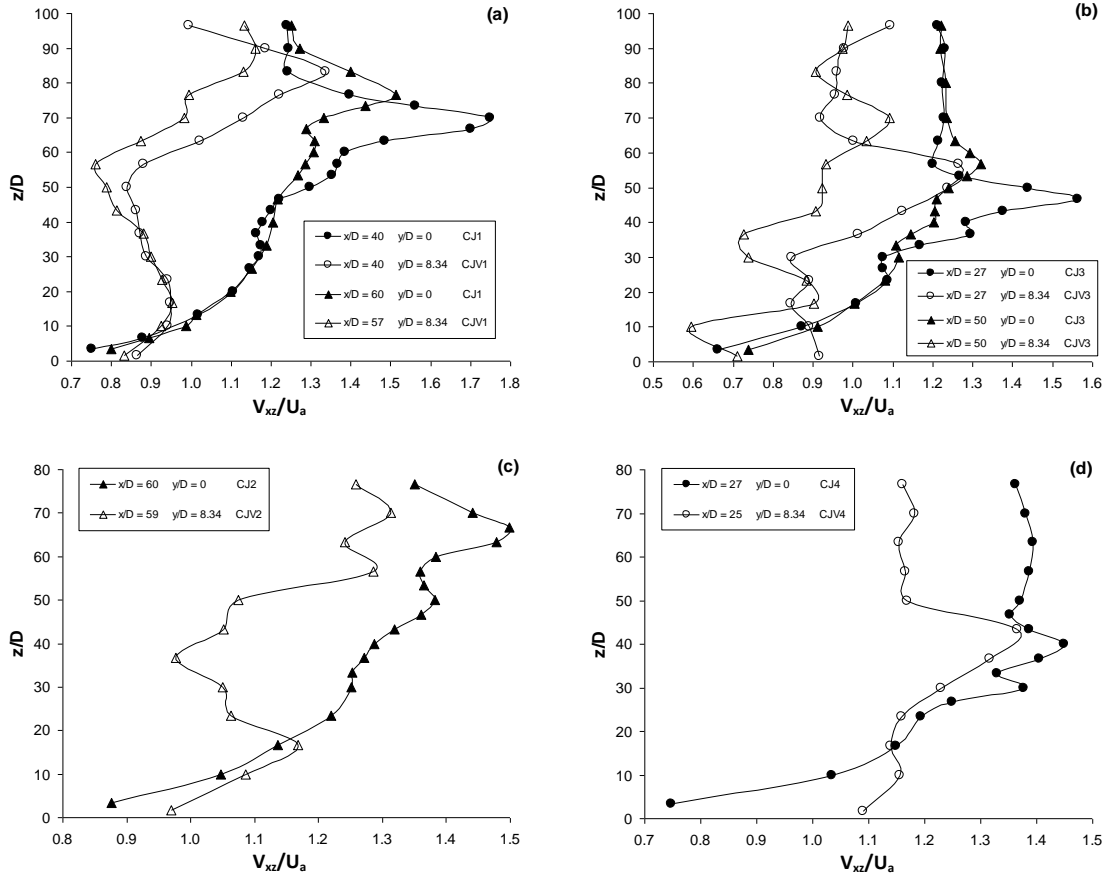


**Fig. 8.** Comparison between the dimensionless velocity profiles  $V_{xz}/U_a$  of jets discharged into the unobstructed and the obstructed channel flows, at different downstream positions  $x/D$ .

The velocity profiles in Fig. 8 clearly show that  $V_{xz}$  experiences two peaks. One peak in the jet wake-like region which is usually a local maximum velocity, while the other one appears in the jet field which is an absolute maximum, corresponding to the jet velocity axis. Both velocity peaks appear on the profiles of runs CJ1 to CJ4 as in runs CJV1 to CJV4. These results are in good agreement with those obtained by Sherif and Pletcher (1989) for round jets in crossflow. In addition, it can be noted that the vertical position  $z/D$  of both peaks increases as  $r_{ja}$  increases. The vertical profiles in Fig. 8 also show that  $V_{xz}$  considerably decreases in magnitude in the obstructed channel (runs CJV1 to CJV4) compared to that in the unobstructed channel (runs CJ1 to CJ4). Close

to the channel bottom,  $V_{xz}$  experiences, however, greater values for runs CJV1 to CJV4. At this region, far away downstream of the jet exit, the ambient flow dominates and the jet effect almost disappears. The slight increase of  $V_{xz}$  with runs CJV1 to CJV4 compared to runs CJ1 to CJ4, at this region, can be explained by the fact that, with emergent vegetation, the mean flow velocity remains almost constant along the vertical, making the bottom surface boundary layer compressed toward the bed (Ben Meftah and Mossa, 2013; Pokrajac and Manes, 2008).

Fig. 9 shows the contour lines of the dimensionless velocity  $V_{xz}/V_\xi$  in the channel cross-section for run CJ1 (jet in unobstructed channel) at two downstream positions  $x/D = 40$  and  $60$ .  $V_\xi$  is defined as the jet velocity axis, i.e., the maximum value of  $V_{xz}$  along the vertical profile in the plane of flow symmetry. Since the jet and the channel flows are symmetric with respect to the plane of flow symmetry ( $y/D = 0$ ), in Fig. 9 we only plot the data of the half cross-section. In Fig. 9, the contour line intervals of the normalized velocity have constant spacing of 0.04. The gray dashed line indicates the lateral position at  $y/D = 8.34$ . The black and semi-black points indicate the locus of the maximum value of  $V_{xz}$  in the plane of flow symmetry ( $y/D = 0$ ) and in the plane at  $y/D = 8.34$ , respectively. In both downstream positions  $x/D = 40$  and  $60$ , Fig. 9 clearly shows the jet kidney-shaped cross-section, developed within the ambient flow (Rajaratman, 1976). As going further downstream from the jet exit, it can be noted that the jet penetrates much more within the ambient flow, increasing significantly its cross-section. These results are in good agreement with several previous studies (e.g., Cortelezzi and Karagozian, 2001; Rajaratman, 1976). Moreover, Fig. 9 obviously indicates that the locus of the peak of  $V_{xz}$  (semi-black point) in the plane at  $y/D = 8.34$  always appears down the jet axis (black point).

With the aim to obtain more information on the interaction between the jet flow, the ambient flow and the array of cylinders, it was useful to deeply analyse the three flow velocity components. Fig. 10 shows the dimensionless streamwise  $U/U_a$ , the spanwise  $V/U_a$  and the vertical  $W/U_a$  velocity profiles for the different runs CJ1 to CJ4 (jet in the unobstructed channel) and CJV1 to CJV4 (jet in the obstructed channel). The velocity profiles, at  $x/D = 26.67, 40, 50$  and  $73.34$ , of runs CJ1 to CJ4 refer to the plane of flow symmetry ( $y/D = 0$ ), while those of runs CJV1 to CJV4 refer to the plane at  $y/D = 1.67$ . Each pair of corresponding runs, carried out in both the unobstructed and the obstructed channel flows and of the same velocity ratio  $r_{ja}$  (see Table 1), are reported in a single figure. In Fig. 10, the vertical coordinate  $z$  is normalized by the channel flow depth  $H$ , instead the jet diameter  $D$ , with the aim to plot all the profiles at the same vertical scale.

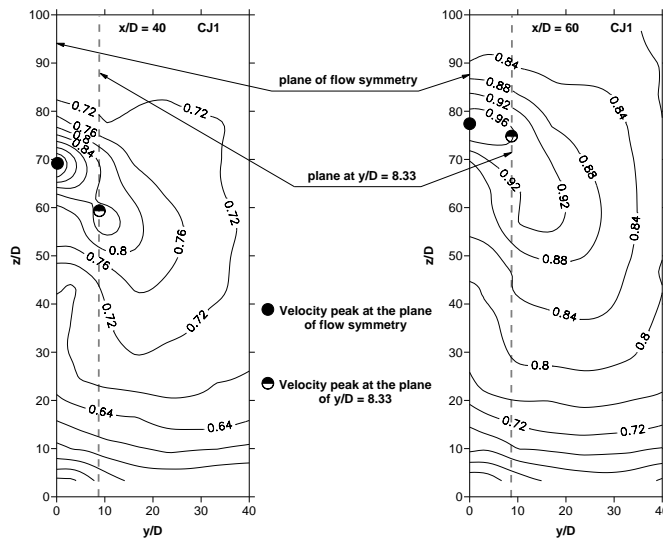


**Fig. 9.** Contour lines of the dimensionless velocity  $V_{xz}/V_\xi$  at the channel cross-section of  $x/D = 40$  and  $60$ , run CJ1.

Fig. 10 indicates that  $U$  almost follows the same profile trend as  $V_{xz}$  (Fig. 8). The absolute maximum of the jet field and the local maximum of the wake-like regions are also clearly shown by the vertical profiles of  $U/U_a$ , which are more pronounced at the downstream position of  $x/D = 26.67$  and 40. At  $x/D = 73.34$ , the two velocity maxima are less pronounced, and the  $U$ -profile tends to almost resemble a classical vertical profile of the mean velocity in an unobstructed channel flow. After reaching its maximum value, in the jet field,  $U$  starts to decrease gradually and gets an almost constant value of order  $1.2U_a$  near the free stream velocity. These results are in complete agreement with those obtained by Sherif and Pletcher (1989) with a velocity ratio  $r_{ja} = 6$ . Fig. 10 shows that  $U$  always almost experiences the smallest magnitudes for runs CJV1 to CJV4 relative to runs CJ1 to CJ4, except at the region close to the channel bottom where  $U$  tends to become slightly greater with runs CJV1 to CJV4, as also observed in Fig. 8. Fig. 10 also indicates that, for runs CJV1 to CJV4, the two velocity maxima of  $U/U_a$  are achieved at higher vertical positions compared to runs CJ1 to CJ4, due to the increase of the jet penetration height.

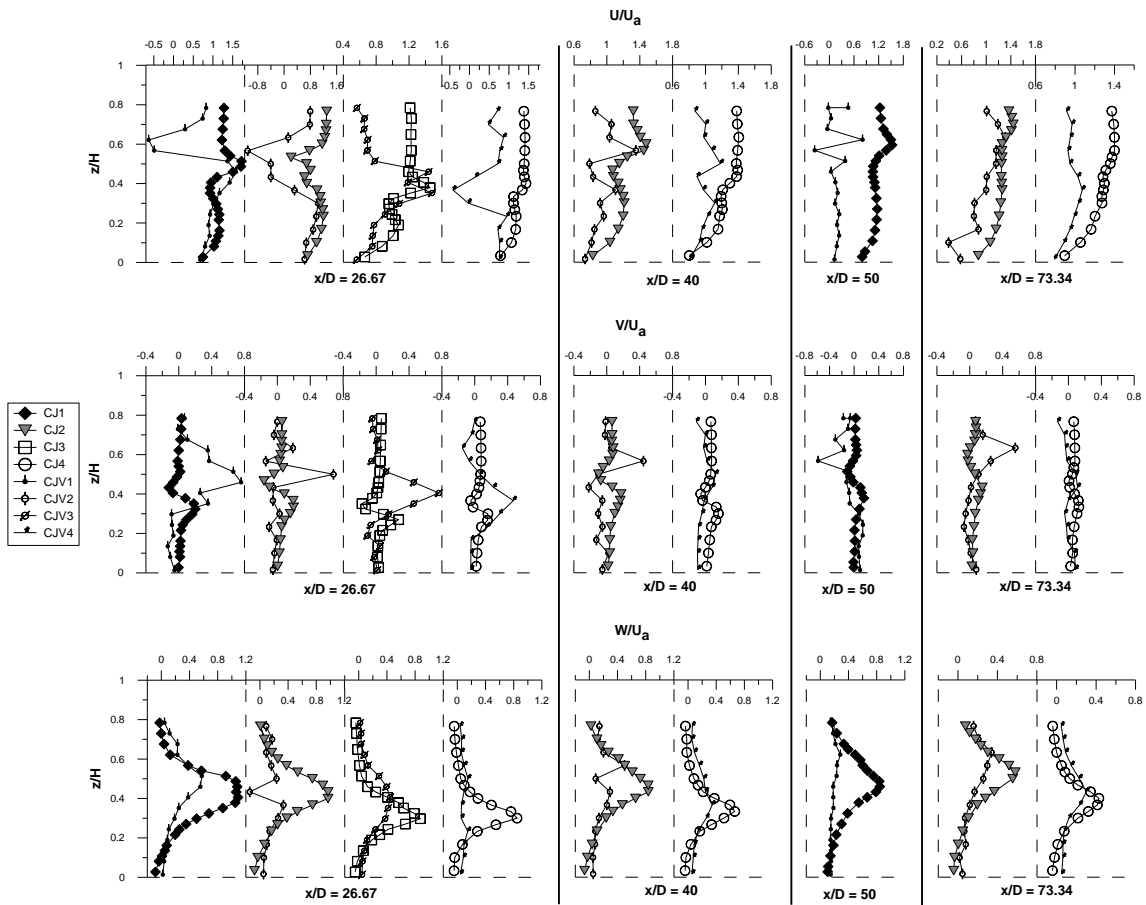


**Fig. 10.** Normalized streamwise  $U/U_a$ , spanwise  $V/U_a$  and vertical  $W/U_a$  velocity profiles for runs CJ1 to CJ4 in the plane of flow symmetry ( $y/D = 0$ ) and for runs CJV1 to CJV4 in the plane at  $y/D = 1.67$ .

Fig. 10 indicates that  $V$  is almost null in the plane of flow symmetry (CJ1 to CJ4). Over a certain distance on the vertical profiles, a kind of a  $S$ -shape region can be observed, in correspondence with the jet flow field. Theoretically,  $V$  should be null everywhere in the plane of flow symmetry, which is not reachable experimentally (Rivero et al., 2001). In the plane at  $y/D = 1.67$ , very close to the plane of flow symmetry,  $V$  shows, in contrast, significant magnitudes with runs CJV1 to CJV4, especially at the level of the jet field. All the profiles show a peak of positive  $V$  at the different downstream positions, except at  $x/D = 50$  where a negative peak occurred. It is worth mentioning that  $x/D = 50$  is a position of a lateral row of cylinders, which implies the interaction of the jet with the disturbed local flow by the rods, as shown in Fig. 7. The sharp increase of  $V$ , observed with runs CJV1 to CJV4, can be explained by the development of the

transversal flow motion caused by the array of cylinders, as clearly shown in Fig. 7. This transversal flow motion surely leads to more lateral spreading of jet within the crossflow.

In contrast to the  $U$ -profile trend,  $W$  shows a drastically different mode of development. It always experiences an absolute maximum below the jet axis, which is in good agreement with that observed by Sherif and Pletcher (1989).  $W$  shows almost similar behaviours for both the jet discharged into the unobstructed channel (runs CJ1 to CJ4) and the jet discharged into the obstructed channel (runs CJV1 to CJV49). For runs CJV1 to CJV4, the  $W$ -profiles undergo some occasional disturbance due to the array effects. In the obstructed channel,  $W$  always peaks at vertical locations higher than in the unobstructed channel, confirming the role of the cylinders array to increase the jet penetration height. At  $x/D = 50$ ,  $W$  significantly reduces for CJV1, undergoing the local effect of the single cylinder. Fig. 10 also depicts that the peak of  $W$  for runs CJV1 to CJV4 is always small (two to three times smaller) compared to that obtained with runs CJ1 to CJ4.

Finally, it can be concluded that the effect of the cylinders/vegetation array on the jet flow is manifested by a reduction of both the jet streamwise and vertical velocity components against an increase of the transversal velocity component, promoting a major lateral spreading of the jet within the crossflow.

As previously mentioned, the velocity measurements in the plane of flow symmetry are of crucial importance in determining some fundamental characteristics of the jet, but they are not sufficient to completely describe a jet in a crossflow. Since the jet is three-dimensional, a more detailed description of the jet requires additional cross-sectional velocity measurements. In the present study, extensive measurements of the field velocity in several cross-sections were carried out for each test. Although most measurements were taken in the one-half channel cross-section of  $y \geq 0$ , some measurements were also taken for  $y < 0$  in order to verify the flow symmetry relative to the vertical-longitudinal-plane at  $y = 0$ , as shown in Fig. 11. Fig. 11 shows the field velocity distribution  $V_{yz}$  (resultant of  $V$  and  $W$  velocity components) in the channel cross-section for run CJ3, at the downstream position  $x/D = 26.67$ . Fig. 11 also illustrates a close-up area of the jet field in order to clearly show its vortical structures. The  $V_{yz}$ -velocity field clearly shows the development of a counter-rotating vortex pair associated with the jet cross-section. This finding is in good agreement with that obtained in previous studies (e.g., Andreopoulos and Rodi; 1984; Cortelezzi and Karagozian, 2001; Rajaratnam, 1976; Richard and Weston, 1978). The CRVP in Fig. 11 confirm that the vertical-longitudinal-plane at  $y = 0$  is a plane of flow symmetry.

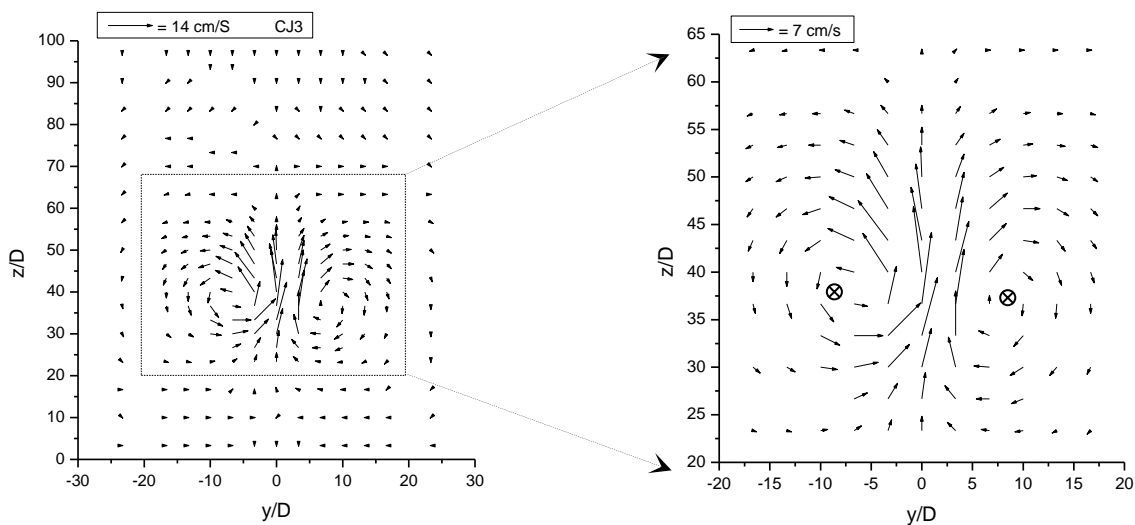


**Fig. 11.** Velocity distribution in the channel cross-section at  $x/D = 26.67$ . The symbol  $\otimes$  represents the vortex centre.

Fig. 12 shows an example of the jet cross-section in both the unobstructed and the obstructed channel flows, at the downstream position  $x/D = 26.67$ . Figs. 12(a) and (b) show the isocontours of

the normalized velocity  $V_{xz}/U_a$  for runs CJ3 and CJV3 in the half channel cross-section of  $y \geq 0$ , respectively. The isocontours presented in Fig. 12(a) exhibit their maximum value at  $y/D = 0$  and clearly show a kidney-shaped jet cross-section. In the obstructed channel, however, as shown in Fig. 12(b), the isocontours undergo complex structures. The familiar kidney-shape of the jet cross-section, observed in the unobstructed channel, disappears and the dominant CRVP break down, due to the array effects, into several random vortices. The vortical structure, observed in Fig. 12(b), occupies a cross-section area greater than the jet cross-section shown in Figure 12(a). This confirms the increase of the jet spreading in the obstructed channel flow, giving rise to substantial increase of the jet dilution within the ambient flow.

Fig. 12(c) shows a vector map of  $V_{yz}$  for run CJV3 in the half channel cross-section ( $y \geq 0$ ) and at the same downstream position  $x/D = 26.67$ . The same vector-scale used in the close-up area of Fig. 11 was also maintained in Fig. 12(c). Comparison between Fig. 11 and Fig. 12(c) clearly shows the notable difference of the flow structures between run CJ3 and run CJV3. The distribution of the velocity vectors in run CJV3 seems extremely random compared to an orderly distribution shown in Fig. 11 for run CJ3. The dominant CRVP, observed in run CJ3, vanishes in run CJV3, giving rise to a disturbed flow field region. Fig. 12(c) shows that, at  $0 < y/D < 7$ ,  $V_{yz}$  tends more toward the transversal direction compared to that observed in CJ3. This clearly explains how the array of cylinders/vegetation affects the jet flow, allowing it to spread more laterally.

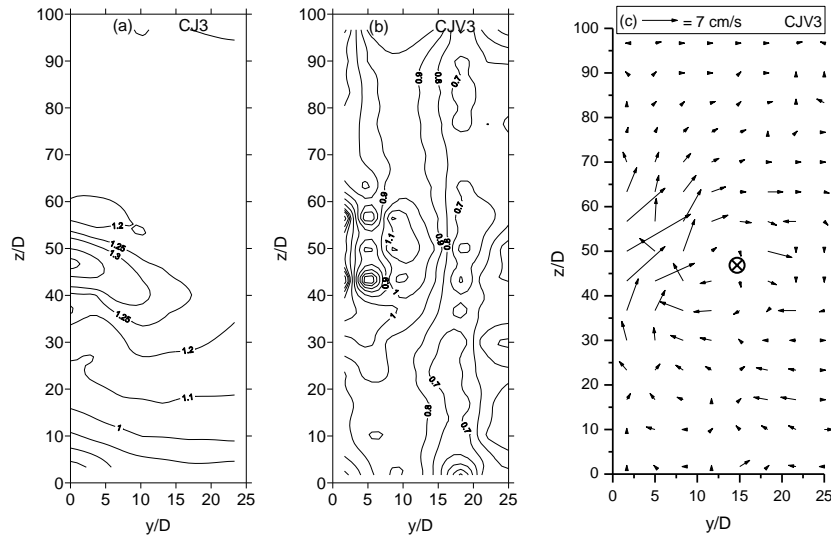


**Fig. 12.** Effects of the array of cylinders on the jet flow structure at the downstream position  $x/D = 26.67$ : (a) and (b) isocontours of  $V_{xz}/U_a$  of runs CJ3 and CJV3, respectively, (c) vector map of  $V_{yz}$  for run CJV3.

## 4. Conclusions

In recent years, numerous experimental and numerical studies have been conducted on vegetated channels, on the one hand, and on turbulent jets discharged into unvegetated crossflows, on the other hand. However, it is observed a lack of information regarding jet discharges into obstructed channels.

Since effluents are mostly discharged into receiving water bodies by pipes, forming single jets, a good knowledge of the interaction between the effluents, the jet characteristics and the receiving environments is required to promote best environmental management practice. The present study was carried out in order to obtain a more thorough understanding of aquatic vegetated-crossflow effects on a round, vertical, turbulent, momentum jet discharged into it. The instantaneous three flow velocity components, within the jet and the ambient flows, were accurately measured in three scenarios. The first scenario concerns a jet discharged into an unobstructed channel flow, with the objective to know the jet structure without vegetation canopy effects. The second scenario

investigates an obstructed channel by an array of cylinders, but without jet, in order to understand the vegetation effects on the main ambient flow. The third scenario combines between the first and the second scenarios, examining a jet discharged into an obstructed channel flow, simulating natural vegetated channel flows.

Analysis of the measured flow velocities through the jet and the ambient flows led to the following results:

- (i) the jets discharged into the unobstructed channel clearly show the development of the familiar counter-rotating vortex pair and the well-known kidney-shape of the jet cross-section, principal characteristics of jets discharged into unobstructed channel flows (Cortelezzi and Karagozian, 2001; Rajaratnam, 1976);
- (ii) the normalized jet axes in the unobstructed channel follow a power-law trend, as shown in Equation (2), which is in complete agreement with several previous studies (e.g., Chochua et al., 2000; Kamotani and Greber, 1972; Margason, 1968; Pratte and Baines, 1967; Richard and Weston, 1978);
- (iii) the rigid emergent vegetation/cylinders significantly affects the ambient flow structures and velocities, giving rise to a substantial increase of the transversal flow motion. Within the emergent array of cylinders, only the longitudinal and the transversal exchange zones are present and the vertical exchange zone vanishes.
- (iv) the rigid emergent vegetation reduces the mean channel velocity, allowing the jet to penetrate higher into the crossflow;
- (v) in the vegetated/obstructed channel, the familiar kidney-shape of the jet cross-section, observed in the unobstructed channel, disappears and the dominant CRVP break down, due to the vegetation effects, into several random vortices;
- (vi) the rigid emergent vegetation reduces both the jet streamwise and vertical velocity components against an increase of the transversal velocity component, promoting a major lateral spreading of the jet within the crossflow.

Finally, it can be concluded that the variation of the flow patterns, caused by an aquatic vegetation canopy, affects the jet mixing process and consequently the dilution of pollutants discharged in receiving water bodies.

## Acknowledgement

This study was carried out at the Hydraulic Laboratory in the Department of Civil, Environmental, Building Engineering and Chemistry of the Technical University of Bari, Italy.

The authors wish to dedicate this manuscript to Prof. Antonio Felice Petrillo on the occasion of his retirement.

## Notation

$a$	Total frontal area (area exposed to the flow) per unit array ( $\text{m}^{-1}$ )
$C_D$	Drag coefficient (-)
$\overline{C_D}$	Bulk drag coefficient (-)
$D$	Jet diameter (m)
$d$	Stem circular cylinder diameter (m)
$Fr_a$	Channel Froude number (-)
$Fr_0$	Initial jet Froude number (-)
$H$	Flow depth (m)
$h$	Vegetation height (m)
$n$	Stem density ( $\text{stem.m}^{-2}$ )
$Re_a$	Channel Reynolds number (-)
$Re_d$	Reynolds number based on the stem diameter (-)
$Re_0$	Initial jet Reynolds number (-)

$r_{ja}$	Initial jet to ambient velocity ratio $U_0/U_a$ (-)
$T$	Water temperature ( $^{\circ}\text{C}$ )
$U, V,$	Streamwise, spanwise and vertical mean velocity, respectively ( $\text{ms}^{-1}$ )
$U_a$	Ambient velocity ( $\text{ms}^{-1}$ )
$U_0$	Initial jet velocity ( $\text{ms}^{-1}$ )
$V_{xy}$	Resultant velocity of $U$ and $V$ in the $xy$ -plane ( $\text{ms}^{-1}$ )
$V_{xz}$	Resultant velocity of $U$ and $W$ in the $xz$ -plane ( $\text{ms}^{-1}$ )
$V_{yz}$	Resultant velocity of $V$ and $W$ in the $yz$ -plane ( $\text{ms}^{-1}$ )
$V_{\xi}$	Resultant velocity at the jet axis ( $\text{ms}^{-1}$ )
$x, y, z$	Longitudinal, lateral and vertical coordinates, respectively (m)
$z_0$	Jet port height (m)
$\Delta S$	Space between stems (m)
$\xi$	Jet axis (m)

## References

- Andreopoulos, J., Rodi, W., 1984. Experimental investigation of jets in a crossflow. *J. Fluid Mech.* 138, 93-127.
- Ben Meftah, M., Davies, P., Malcangio, D., Mossa, M., Petrillo, A., 2004a. Turbulence of vertical round buoyant jets in a crossflow. *Proceedings of the Second International Conference on Fluvial Hydraulics, IAHR River Flow 2004, Naples (Italy), June 23-25, 2004. II*, 1167-1174.
- Ben Meftah, M., Mossa, M., 2013. Prediction of channel flow characteristics through square arrays of emergent cylinders. *Phys. Fluids* 25(4), 045102,1-21.
- Ben Meftah, M., De Serio, F., Mossa, M., 2014. Hydrodynamic behavior in the outer shear layer of partly obstructed open channels. *Phys. Fluids* 26(6), 065102, 1-19.
- Chochua G., Shyy, W., Thakur, S., Brankovic, A., Lienau, J., Porter, L., Lischinsky, D., 2000. A computational and experimental investigation of turbulent jet and crossflow interaction. *Numer. Heat Tr. A-Appl.* 38, 557-572.
- Cortelezzi, L., Karagozian, A.R., 2001. On the formation of the counter-rotating vortex pair in transverse jets. *J. Fluid Mech.* 446, 374-373.
- Daly, H.E., 1990. Toward some operational principles of sustainable development. *Ecological Economics* 2, 1-6.
- Eroglu, A., Breidenthal, R.E., 1998. Exponentially acceleration jet in crossflow. *AIAA J.* 36(6), 1002-1009.
- Fairbanks, J.D., 1998. Velocity and turbulence characteristics in flows through rigid vegetation. MS thesis (Virginia Polytechnic Institute & State University).
- Fischer, H.B., List, E.J., Koh, R.C.Y., Imberger, J., Brooks N.H., 1979. *Mixing in inland and coastal waters.* Academic Press, New York.
- Fric, T.F., Roshko, A., 1994. Vortical structure in the wake of a transversal jet. *J. Fluid Mech.* 279, 1-47.
- Ghisalberti, M., Nepf, H.M., 2004. The limited growth of vegetated shear layers. *Water Resour. Res.* 40(7), W07502, 1-12.
- Hasselbrink, J.E.F., Mungal, M.G., 2001. Transverse jets and jet flames: Part1. Scaling laws for strong transverse jets. *J. Fluid Mech.* 443, 1-25.
- Jirka, G.H., Harleman, D.R.F., 1979. Stability and mixing of a vertical plane buoyant jet in confined depth. *J. Fluid Mech.* 94, 275-304.
- Kamotani, Y., Greber, I., 1972. Experiments on a turbulent jet in a crossflow. *AIAA J.* 30(11), 1425-1429.
- Kang, S., 2003. Characteristics of flow over two circular cylinders in a side-by-side arrangement at low reynolds numbers. *Phys. Fluids* 15(9), 2486-2498.
- Keffer, J.F., Baines, W.D., 1963. The round turbulent jet in a cross wind. *J. Fluid Mech.* 15, 481-

- Lightbody, A.F., Nepf, H.M., 2006. Prediction of near-field shear dispersion in an emergent canopy with heterogeneous morphology. *Environ. Fluid Mech.* 6(5), 477-488.
- Margason, R.J., 1968. The path of a jet directed at large angles to a subsonic stream. N.A.S.A., TN.D. 4919, Langley Research Center, Hampton, Virginia.
- Morton, B.R., Ibbetson, A., 1996. Jets deflected in a crossflow. *Exp. Therm. Fluid Sci.* 12, 112-133.
- Mossa, M., 2004a. Experimental study on the interaction of non-buoyant jets and waves. *J. Hydraul. Res.* 42(1), 13-28.
- Mossa, M., 2004b. Behavior of non-buoyant jets in a wave environment. *J. Hydraul. Eng-ASCE* 130(7), 704-717.
- Muppidi, S., Mahesh, K., 2007. Direct numerical simulation of round turbulent jets in crossflow. *J. Fluid Mech.* 574, 59-84.
- Nepf, H.M., Sullivan, J.A., Zavistoski, R.A., 1997. A model for diffusion within an emergent plant canopy. *Limnol. Oceanogr.* 42(8), 85-95.
- Nepf, H.M., 1999. Drag, turbulence and diffusion in flow through emergent vegetation. *Water Resour. Res.* 35(2), 479-489.
- Nepf, H.M., Vivoni E.R., 2000. Flow structure in depth-limited, vegetated flow. *J. Geophys. Res.* 105(C12), 28547-28557.
- Nepf, H.M., 2004. The ecogeomorfology of tidal marshes: Vegetated flow dynamics. Coastal and Estuarine Volume. Copyright 2004 by the American Geophysical Union.
- New, T.H., Lim, T.T., Luo, S.C., 2006. Effects of jet velocity profiles on a round jet in cross-flow. *Exp. Fluids* 40, 859-875.
- Pathak, M., Dewan, A.A., Dass, A.K., 2006. Computational prediction of a slightly heated turbulent rectangular jet discharged into a narrow channel crossflow using two different turbulence models. *Int. J. Heat Mass Tran.* 49, 3914-3928.
- Poggi, D., Katul, G.G., 2008. The effect of canopy roughness density on the constitutive components of the dispersive stresses. *Exp. Fluids* 45, 111-121.
- Poggi, D., Porporato, A., Ridolfi, L., Albertson, J.D., Katul, G.G., 2004. The effect of vegetation density on canopy sub-layer turbulence. *Boundary-Layer Meteorol.* 111, 565-587.
- Pokrajac, D., Manes, C., 2008. Interface between turbulent flows above and within rough porous walls. *Acta Geophysica* 56(3), 824-844.
- Pratte, B.D., Baines W.D., 1967. Profiles of the round turbulent jet in a crossflow. *J. Hydr. Eng. Div.-ASCE, Proceeding of the American Society of Civil Engineers*, 92(HY6), 53-64.
- Quinn, W.R., 2006. Upstream nozzle shaping effects on near field flow in round turbulent free jets. *Eur. J. Mech. B-Fluid*, 25, 279-301.
- Raupach, M.R., Thom, A.S., 1981. Turbulence in and above plant canopies. *Ann. Rev. Fluid Mech.* 13, 97-129.
- Rajaratnam, N., 1976. *Turbulent jets*. Elsevier Scientific Publishing Company, Amsterdam, Oxford, New York.
- Richard, L., Weston, R.P., 1978. Induced velocity field of a jet in a crossflow. NASA Technical Paper 1087.
- Rivero, A., Ferré, J.A., Giralte, F., 2001. Organized motions in a jet in crossflow. *J. Fluid Mech.* 444, 117-149.
- Sherif, S.A., Pletcher, R.H., 1989. Measurements of the flow and turbulence characteristics of round jets in crossflow. *J. Fluids Eng.* 111, 165-171.
- Smith, S.H., Mungal, M.G., 1998. Mixing, structure and scaling of the jet in crossflow. *J. Fluid Mech.* 357, 83-122.
- Tanino, Y., Nepf H.M., 2008. Laboratory investigation of mean drag in a random array of rigid, emergent cylinders. *J. Hydraul. Eng.* 134(1), 34-41.
- Toffolon, M., Serafini, M., 2013. Effects of artificial hypolimnetic oxygenation in a shallow lake. Part 2: Numerical modelling. *J. Environ. Manage.* 114, 530-539.

- Tsujimoto, T., Kitamura, T., Okada, T., 1992. Turbulent open-channel flow over bed covered by rigid vegetation. *J. Hydrosoci. Hydr. Eng.* 10(2), 13-25.
- White, B.L., Nepf, H.M., 2007. Shear instability and coherent structures in shallow flow adjacent to a porous layer. *J. Fluid Mech.* 593(12), 1-32.
- Williamson, C.H.K., 1985. Evolution of a single wake behind a pair of bluff-bodies. *J. Fluid Mech.* 159, 1-18.
- Wilson, N.R., Shaw R.H., 1997. A higher order closure model for canopy flow. *J. Appl. Meteorol.* 16, 1197-1205.
- Worcester, S., 1995. Effects of eelgrass beds on advection and turbulent mixing in low current and low shoot density environments. *Mar. Ecol.: Prog. Ser.* 126, 223-232.
- Yang, W.C., Hwang, R.R., 2001. Vertical buoyant jets in a linearly stratified ambient cross-stream. *Environ. Fluid Mech.* 1, 235-256.
- Zavistoski, R.A., 1994. Hydrodynamic effects of surface piercing plants. MS thesis (MIT. Cambridge, MA).